Annals of Biomedical Engineering, Vol. 45, No. 3, March 2017 (© 2016) pp. 761–774
DOI: 10.1007/s10439-016-1731-2

Effects of Biowastes Released by Mechanically Damaged Muscle Cells on the Propagation of Deep Tissue Injury: A Multiphysics Study

YIFEI YAO,[1] LUCAS XIAN DA ONG,[1,2] XIAOTONG LI,[1] KINLUN WAN,[1] and ARTHUR F. T. MAK[1,3]

[1]Division of Biomedical Engineering, The Chinese University of Hong Kong, Hong Kong SAR, China; [2]Department of Biomedical Engineering, National University of Singapore, Singapore, Singapore; and [3]Division of Biomedical Engineering, The Chinese University of Hong Kong, Rm. 429, Ho Sin Hang Engineering Building, Shatin, N.T., Hong Kong SAR, China

(Received 24 May 2016; accepted 7 September 2016; published online 13 September 2016)

Associate Editor Karol Miller oversaw the review of this article.

Abstract—Deep tissue injuries occur in muscle tissues around bony prominences under mechanical loading leading to severe pressure ulcers. Tissue compression can potentially compromise lymphatic transport and cause accumulation of metabolic biowastes, which may cause further cell damage under continuous mechanical loading. In this study, we hypothesized that biowastes released by mechanically damaged muscle cells could be toxic to the surrounding muscle cells and could compromise the capability of the surrounding muscle cells to withstand further mechanical loadings. *In vitro*, we applied prolonged low compressive stress (PLCS) and short-term high compressive stress to myoblasts to cause cell damage and collected the biowastes released by the damaged cells under the respective loading scenarios. *In silico*, we used COMSOL to simulate the compressive stress distribution and the diffusion of biowastes in a semi-3D buttock finite element model. *In vitro* results showed that biowastes collected from cells damaged under PLCS were more toxic and could compromise the capability of normal myoblasts to resist compressive damage. *In silico* results showed that higher biowastes diffusion coefficient, higher biowastes release rate, lower biowastes tolerance threshold and earlier timeline of releasing biowastes would cause faster propagation of tissue damage. This study highlighted the importance of biowastes in the development of deep tissue injury to clinical pressure ulcers under prolonged skeletal compression.

Keywords—Multiphysics, Toxins diffusion, Muscle cell damage, Tissue mechanics, Deep tissue injury.

INTRODUCTION

Pressure ulcer is tissue damage under prolonged mechanical loading. Persons with spinal cord injury confined to seats and other immobile patients confined to beds are likely to suffer from pressure ulcers.[1,4,7] There are, generally speaking, two forms of pressure ulcers, superficial ulcers and deep tissue injury (DTI).[1,39] DTI can develop into extensive ulceration fast and are more difficult to prevent and treat than superficial ulcers.[3] Muscle tissues around skeletal prominences are highly susceptible to excessive internal stresses and strains caused by skeletal and epidermal loadings.[43,54] Tissue compression beyond certain thresholds can directly cause tissue necrosis leading to DTI. Excessive compressive deformation can cause skeletal muscle cell necrosis.[5,6,15,35] The duration that muscle cells can tolerate a given compression depends on the compressive stress level.[65] High compressive stress can cause muscle cell damage in very short time and low compressive stress, if prolonged, can also cause cell damage. The lymphatic system removes the normally released biowastes and excess tissue fluid from the interstitial space to the circulation. Tissue compression can potentially compromise lymphatic transport and cause accumulation of metabolic biowastes and toxins released from the damaged tissues, which might contribute to further tissue damage.[25,42,49]

If the mechanical loading exceeds a certain threshold, the muscle cells may undergo apoptosis or necrosis,[15,34,51,65] leading to tissue failure. Apoptosis, which is programmed cell death, has been shown as a result of mechanical stress in muscle cells.[8,29] Intracellular caspases known as the effectors of apoptosis could be induced by mechanical force.[22] When the intact cell membrane was compromised under compression, the caspases and other apoptotic agonists might be released from the damaged cell. Cytokines like tumor necrosis factors (TNF) and interleukins can be secreted by muscle cells in various situations.[32,46,47]

Address correspondence to Arthur F. T. Mak, Division of Biomedical Engineering, The Chinese University of Hong Kong, Rm. 429, Ho Sin Hang Engineering Building, Shatin, N.T., Hong Kong SAR, China. Electronic mail: arthurmak@cuhk.edu.hk

TNF-α possesses multiple biology functions in different cell types.[61] Mechanical loading and injury can induce human skeletal muscle cells to release cytokines that can influence neutrophil responses.[57] Stressed or injured muscle cells produce TNF-α acting as a local mediator.[18,31] The increase of plasma membrane permeability under mechanical stress[52,53] can allow a massive influx of Ca^{2+} that can increase mitochondrial generation of reactive oxygen species (ROS).[21] The caspases, cytokines and ROS might be among the metabolic biowastes and toxins being accumulated in compressed tissues. Few literatures reported on the effects of the biowastes released from the mechanically damaged muscle cells on the normal cells. Such effects could be important to the propagation of DTI.

Cytokines like TNF-α can induce TNF receptors in skeletal muscle cells[67] and suppress protein synthesis.[14] Furthermore, TNF-α can also induce changes in the mechanical properties of cells[24] and reorganization of actin cytoskeleton.[62] Caspases could affect the mechanical properties of cells by cytoskeletal remodeling.[48,55] ROS could also affect the cell mechanical responses.[63,65] Accumulated biowastes secreted from damaged muscle cells might affect the mechanical properties of the surrounding muscle cells, causing more cells to be damaged under subsequent mechanical loadings.

Finite element (FE) modeling has been used in analyzing the internal conditions related to the etiology of DTI.[38,44,60,64] Linder-Ganz *et al.*[37] first established the human buttock FE model based on the morphological data from open MRI on specific seated human subjects. A semi-3D FE model representing the cross section of a human buttock seated on a cushion was developed in this study based on the work of Linder-Ganz and Gefen[36] and Xiao *et al.*[64] The above models were used to describe how the high stresses around the ischial tuberosity (IT) caused the muscle tissue damage propagation from the deep tissue to the skin. Multiphysics simulation was used in many biomechanically coupled problem such as the coupling between fluid flow and structural deformation on aortic valve functions,[23] electrochemohydraulic transports in cortical bone,[26] chemoelectromechanical activities in skeletal muscle,[20] and the coupling of temperature and flow field in arteries.[30] Multiphysics modeling was a good tool to study the diffusion of biowastes in the structurally deformed muscle tissue. Multiphysics models of cellular-scale transport in deformed muscles,[50] oxygen diffusion in skeletal muscle cells under compressive deformation[28] and intracellular oxygen level of muscle cells under stretching[27] focused on the roles of cellular chemical diffusion in DTI. Relatively speaking, little attention has been given to modeling the coupled effects of tissue-scale mechanical loading and biowastes diffusion on muscle damage propagation in DTI.

We hypothesized that biowastes released by mechanically damaged muscle cells could be toxic to other muscle cells in the neighborhood and would compromise the capability of the surrounding muscle cells to withstand compressive damage. We built multiphysics FE model to reveal the importance of biowastes toxification in the etiology of DTI.

MATERIALS AND METHODS

Cell Culture

C2C12 mouse skeletal myoblasts (ATCC, Manassas, USA) were grown in tissue culture dishes (SPL Lifesciences, Korea) with growth medium consisting of high-glucose Dulbecco's Modified Eagle Medium (Gibco, Life Technologies, USA), 10% fetal bovine serum (Gibco, Life Techologies, USA) and 1% Penicillin–Streptomycin (Gibco, Life Technologies, USA). The myoblasts were trypsinized by 0.25% Trypsin–EDTA (1×, Gibco, Life Technologies) for the cell passage process every three days to maintain the continuous passage. The myoblasts in this study were of passage 15–19. Myoblasts were seeded in low density (~2×10^4 cells cm^{-2}) and cultured in monolayer in six-well plates and in 35 mm diameter tissue culture dishes (SPL Lifesciences, Korea) in a 37 °C, 5% CO_2 humidified incubator for two days. The monolayers were about 80% confluent at the time of the experiments.

Collection of Biowastes

Two kinds of agarose gels were prepared by dissolving 0.5% (w/v) and 2% (w/v) agarose (Biosharp, Hefei, China) powder in Dulbecco's phosphate-buffered saline (PBS, 1×, Gibco, Life Technologies) at 100 °C. The agarose solution was dispensed into the 35 mm petri dish and then cooled in room condition to form a 3 mm thick gel layer. A cylindrical gel of thickness 3 mm and diameter 14.8 mm was cut out and placed over a monolayer of myoblasts.

The compressive stress applied on the monolayer of myoblasts was provided by a Mach-1™ micromechanical system (Biomomentum Inc) at 37 °C and 5% CO_2. A 30% uniaxial compression of the agarose gel was conducted in the Mach-1™ micromechanical testing system with a flat platen of diameter 25.4 mm. After the flat platen reached the top surface of the gel, 1 mL of culture medium was added into the tissue culture dish. About 150 Pa compressive stress was generated on the myoblasts under the 0.5% agarose gel

for 15 min or 3 h with 30% gel compressive strain. About 3000 Pa compressive stress was generated on the myoblasts under the 2% agarose gel for 15 min or 3 h by 30% gel compressive strain. The details of this loading methodology was reported earlier.[65]

After compression with the specific intensity and duration, 1 mL of the culture medium containing the biowastes secreted by the damaged myoblasts was collected. Four groups of biowastes were collected—namely those from cells damaged under (i) prolonged low compressive stress (PLCS, i.e., 150 Pa for 3 h), (ii) prolonged high compressive stress (PHCS, i.e., 3000 Pa for 3 h), (iii) short-term high compressive stress (SHCS, i.e., 3000 Pa for 15 min) and (iv) short-term low compressive stress (SLCS, i.e., 150 Pa for 15 min).

Cell Toxicity Test

Myoblasts in six-well plates were cultured for 1, 3 and 5 h in the biowastes collected from the mechanically damaged myoblasts (SHCS and PLCS) as the treated groups. Myoblasts cultured in fresh culture medium were used as control. Propidium Iodide (PI) (Sigma, USA) at 10 μg mL^{-1} was used to stain the nuclei of the damaged cells with red fluorescence for cell damage assessment. Fluorescence microscopy was performed in an inverted microscope (ECLIPSE Ti, Nikon). A G-2B filter was used to capture the red fluorescence of PI. Images were taken at $\times$100 magnification with a CCD camera (DS-Fi1c-L3, Nikon Digital Sight). PI stained nuclei were counted using the ImageJ 1.46r (NIH). At the end of the experiment, the total number of the myoblasts in each well was counted after fixing the cells with 4% paraformaldehyde together with 0.1% Triton X-100 and PI staining. The toxicity of the biowastes was measured by calculating the percentage of PI-stained myoblasts in the mere presence of the biowastes to the total number of myoblasts in each well. One-way Analysis of variance (ANOVA) at 0.05 level of significance was used to test the significant difference in toxicity among the biowastes treatments.

Compressive Stress Damage Threshold

The method to determine the compressive stress damage threshold described in Yao *et al.*[65] was used in this study. Briefly recapped, the myoblasts monolayer immerged in 1 mL of media with biowastes was covered under a 3 mm-thick agarose gel. The gel was loaded by a half-spherical indenter of 6.38 mm diameter in a Mach-1^{TM} micromechanical testing system at 37 °C with 5% CO_2 at a rate of 0.01 mm s^{-1} until the deformation at the center of the gel reached 50%. The radially varying compressive stress field generated by the indentation at the bottom surface of the gel was assumed effectively acting on the top surface the monolayer of myoblasts. Myoblasts treated by the SHCS biowastes were indented for 30, 70, 140, 160, 180 and 300 min and myoblasts treated by the PLCS biowastes were compressed for 15, 30, 50, 70, 100, 140 and 180 min. Myoblasts treated by the PHCS and SLCS biowastes were also compressed for 70 min for two-way ANOVA to determine the main experimental factor associated with the biowastes causing significant changes on the compressive damage threshold. The compressive stress profile applied on the myoblasts was adopted from the published data in Yao *et al.* simulating the same experimental configuration.[65] PI was used to assess the spatial profiles of percentages of cells dead after indentation. The damage threshold of myoblasts was determined by the correlation between the cell damage percentage profile and the compressive stress profile acting on the myoblasts monolayer. With the criteria that the percentage cell damage within the damaged threshold circle was at least 3 times that in the peripheral region, the relation between the compressive damage threshold and the indentation duration was determined. Nonparametric ANOVA was performed using Kruskal–Wallis test with 0.05 level of significance to test the effects of the two kinds of biowastes treatments. The experimental data on the compressive stress threshold vs loading duration for each treatment of biowastes were fitted with a decreasing Boltzmann-type sigmoid function first developed by Linder-Ganz *et al.*:[34]

$$\sigma(t) = \frac{K}{1 + e^{\alpha(t - t_0)}} + C \tag{1}$$

where K, t_0, α and C are determined by least square curve-fitting; and $\sigma(t)$ is the compressive stress threshold.

Multiphysics Finite Element Modeling

The biowastes generated by the mechanically damaged muscle cells could diffuse in the muscle tissue and lower the capability of the surrounding muscle cells to resist against compression damage by lowering the compressive damage threshold of the cells. Meanwhile, the biowastes released from the mechanically damaged cells may also depend on the loading scenarios. The coupling between the solid mechanics and the chemical diffusion of biowastes in the tissue level was modeled on the COMSOL Multiphysics platform. To simulate the damage propagation of DTI in the muscle tissues, a semi-3D FE cross-sectional model of a buttock seated on a cushion was developed based on the work of Linder-Ganz and Gefen[36] and the subsequent work of

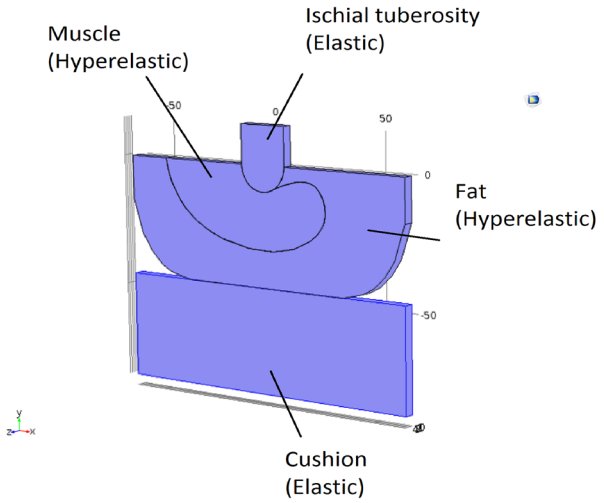

FIGURE 1. Finite element model (COMSOL) of a human buttock (half) on an elastic cushion.

Xiao *et al.*[64] We also adopted the damage laws to determine the tissue damage by following the concepts in the original work of Linder-Ganz and Gefen.[36] As shown in Fig. 1, the buttock FE model consisted of four parts: IT, muscle, fat and skin (as one part), and cushion. The slice thickness of all the parts was set as 4 mm. All the parts were meshed with tetrahedral elements totaling 21,621 in number. Unstructured quadratic tetrahedral elements were meshed in the Solid Mechanics module and unstructured linear tetrahedral elements were meshed in the Transport of Diluted Species module for the chemical diffusion of biowastes.

The elastic moduli of IT and cushion was set as 7 GPa[12] and 1 MPa[64] respectively, with Poisson's ratio $v = 0.3$. Muscle and fat-skin layers were assumed to be hyperelastic. The Poisson's ratios of muscle and fat-skin were assumed to be 0.49, as nearly incompressible. The Neo–Hookean strain energy potential for hyperelasticity was in the following form:

$$U_{\text{neo}} = \frac{1}{2}G(\bar{I}_1 - 3) + \frac{1}{2}K(J_{\text{el}} - 1)^2 \tag{2}$$

where U is the strain energy per unit reference volume; J_{el} is the elastic volume ratio; $\bar{I}_1$ is the first deviatoric strain invariant defined as:

$$\bar{I}_1 = \bar{\lambda}_1^2 + \bar{\lambda}_2^2 + \bar{\lambda}_3^2 \tag{3}$$

$\bar{\lambda}_i$ are the deviatoric principal stretches $\bar{\lambda}_i = J^{-\frac{1}{3}}\lambda_i$; λ_i are the principal stretches; J is the total volume ratio; G is the long-term shear modulus as we only consider the equilibrium minimum principal stress and K is the bulk modulus calculated given the shear modulus and Poisson's ratio using the following equation:

$$v = \frac{3(K/G) - 2}{6(K/G) + 2} \tag{4}$$

The long-term shear modulus G was taken to be 600 Pa for the muscle layer[45] and 143 Pa for the fat-skin layer.[9,10,17,56,64] The bulk modulus K was calculated to be 29.80 kPa for the muscle layer and 7.10 kPa for the fat-skin layer. The nodes at the bottom of the cushion were fixed in all directions. The penalty method was used for the contact pressure at all the interfaces between different parts of the model. The contact pressure penalty factor was taken to be 2 MPa m^{-1} between cushion and fat-skin, 6 MPa m^{-1} between fat-skin and IT, 19 MPa m^{-1} between muscle and IT as well as between muscle and fat-skin. Displacement boundary condition being free in-plane and fixed out-of-plane was applied at both the anterior and posterior surfaces of all the parts. A displacement of 9 mm was applied on the superior surface of IT.[33,37,41]

The transport of biowastes generated by the damaged muscle cells through the undeformed skeletal muscle tissue was modeled in COMSOL by the following chemical diffusion equation:

$$\frac{\partial C}{\partial t} + \nabla \cdot (-D\nabla C) = R_C \tag{5}$$

where C is the concentration of the biowastes, R_C is the release rate of biowastes from damaged muscle cells, and D is the diffusion coefficient of the biowastes in muscle tissue. Temperature was assumed constant and uniform. For parametric analysis, D was allowed to range from 10^{-10} to 10^{-7} m^2 s^{-1} with 10^{-9} m^2 s^{-1} as the reference setting.[2,11,19,58,59] Muscle cells remain intact when the compressive stress and the loading duration were below the compressive damage stress-duration threshold curve, i.e. within the safe region. The region above the compressive damage stress-duration threshold curve is referred as the damage region, where muscle cells will be mechanically damaged. When the muscle cells are in the safe region, $R_C = 0$, which means there are no biowastes released from the cells. When the muscle cells are in the damage region, R_C becomes non-zero, ranging from 10^{-7} to 10^{0} mol m^{-3} s^{-1} for parametric analysis with 10^{-6} mol m^{-3} s^{-1} as the reference setting. We assumed the damaged cells could continuously release biowastes at a certain rate only after loading duration t_0 as timeline of releasing biowastes which ranging from 30 to 180 min with 120 min as the reference setting. The release rate of biowastes from the damaged muscle cells was governed by the following equation:

$$R_C = \begin{cases} R & \text{when } \sigma_{33} > \sigma_t \text{ and } t > t_0 \\ 0 & \text{Otherwise} \end{cases} \tag{6}$$

where σ_{33} is the minimum principal stress in the muscle tissue; σ_t is the compressive stress damage threshold of muscle cells; and t is the loading duration in the unit of minute. The compressive damage stress-duration threshold curve determined the damage of muscle cells. For normal myoblasts, the threshold curve was reported to take the following form:[65]

$$\sigma_N = \frac{340}{1 + e^{0.118(t-160.3)}} + 8.95 \quad (7)$$

σ_N is the compressive stress damage threshold in the unit of pascal. We assumed the compressive damage stress-duration threshold of muscle tissues was similar to that of the myoblasts. From the *in vitro* experimental results reported later, we could represent the compressive damage stress-duration threshold of the myoblasts after the treatment of biowastes as σ_B for all concentration of biowastes. The compressive stress damage threshold for the muscle tissues was defined as:

$$\sigma_t = \begin{cases} \sigma_N & \text{when } C < C_t \\ \sigma_B & \text{when } C \geq C_t \end{cases} \quad (8)$$

where C_t is the chemical damage threshold of muscle cells for biowastes effect. For parametric analysis, C_t was allowed to range from 0 to 10^{-3} mol m^{-3} with 0 mol m^{-3} as reference setting. The biowastes can affect normal muscle cells when its concentration gets above a certain threshold C_t. The distribution of minimum principal stress in the muscle layer and the diffusion of biowastes could be simulated as coupled processes of mechanical deformation and chemical diffusion. The solid mechanics module and biowastes diffusion module are one-way coupled in COMSOL. The diffusion equation was solved in the undeformed geometry with linear tetrahedral elements and the generation of the chemicals was based on the compressive stress results in the solid mechanics module. The diffusion coefficient of the biowastes was independent on the deformation results in the solid mechanics module. The propagation of muscle damage was presented by the percentage of damaged muscle tissue volume calculated based on the compressive stress damage threshold σ_t at each time point. The release rate of biowastes from damaged cells, the chemical damage threshold for biowastes, the diffusion coefficient of biowastes in muscle tissue and timeline of releasing biowastes were parametrically analyzed to show how these factors may influence the propagation of muscle damage.

RESULTS

Biowastes Toxicity

Normal myoblasts were treated for 1, 3, and 5 h with the PLCS biowastes. Comparing the percentages of cells damaged, two-way ANOVA showed significant difference between the PLCS group and the non-treated control group ($p < 0.05$) (Fig. 2a). This showed that the biowastes released by muscle cells damaged under chronic mechanical loading showed significant toxicity to other normal muscle cells. The biowastes treatment duration did not exhibit statistically significant effects among the three treatment durations.

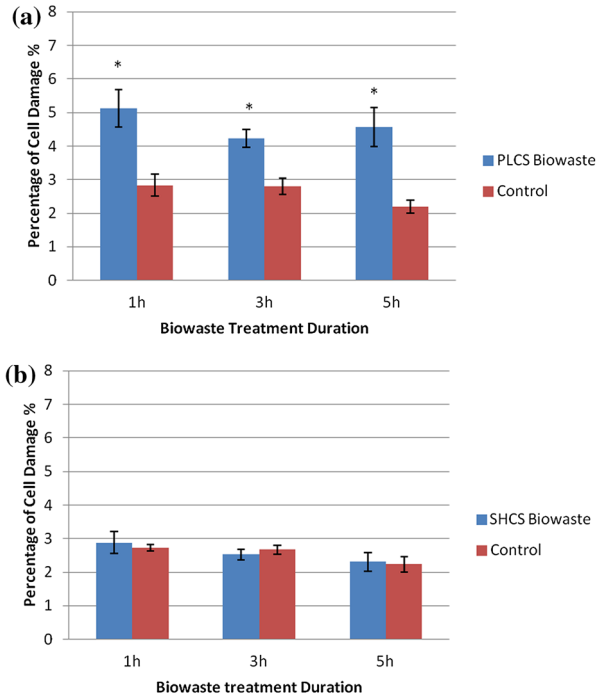

FIGURE 2. (a) Percentages of myoblasts dead after treatments with PLCS biowastes for 1, 3, and 5 h showed significant increases compared to those in the control, indicating the toxicity of the PLCS biowastes. (*$p < 0.05$). (b) Percentages of myoblasts dead after treatments with SHCS biowastes for 1, 3, and 5 h showed no significant differences compared to those in the control, indicating the non-toxicity of the SHCS biowastes.

Normal myoblasts were treated for 1, 3, and 5 h with the SHCS biowastes. Comparing the percentages of cell damaged in the SHCS group with those in the non-treated group, two-way ANOVA showed no significant difference between the two groups ($p > 0.05$) (Fig. 2b). The statistical power of 0.8 was satisfied with a sample size of 3 with type I error less than 0.05 for two-tailed test for the three biowastes treatment durations. This showed that there was no significant lethal effect of the biowastes released by cells acutely damaged under brief exposure to very high stress.

Damage Stress Threshold

The typical spatial profiles of the percentage cell damage in the PLCS and SHCS groups were shown in Fig. 3a. The extent of cells damaged expanded with

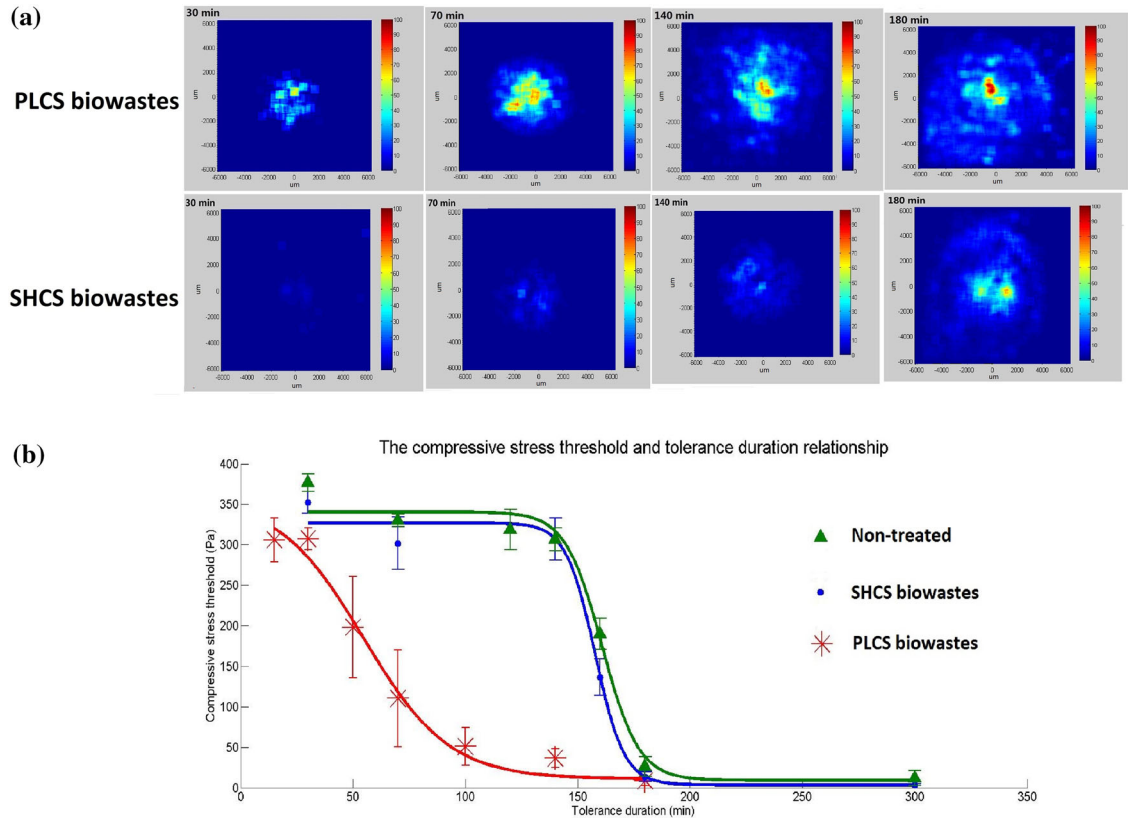

FIGURE 3. (a) Percentages of myoblasts damaged under indentation after PLCS and SHCS biowastes treatments. Results were derived from the PI fluorescent images taken after different indentation durations. (b) The relationships between the compressive stress thresholds and the tolerance durations of myoblasts with PLCS and SHCS biowastes treatments, as compared to myoblasts without pre-treatment with PLCS/SHCS biowastes.[64] Curve-fitted parameters are listed in Table 2.

TABLE 1. The peak percentages of myoblasts damaged in the PLCS and the SHCS biowastes treated groups as compared to the non-treated myoblasts[64] for various indentation durations.

Indentation duration (min)	30 (%)	70 (%)	140 (%)	180 (%)
Non-treated myoblasts	14.5	19.4	26.2	73.4
PLCS biowastes treated myoblasts	52.8	73.2	83.1	95.5
SHCS biowastes treated myoblasts	12.2	21.3	28.4	58.6

increasing indentation duration. Around the center of the indented area, longer loading duration led to higher percentages of cells damaged in both groups. (Table 1).

The relationship between the compressive stress threshold and the tolerance duration of PLCS and SHCS biowastes treated cells were shown in Fig. 3b. For the indentation durations of 30, 70, and 140 min, the compressive stress thresholds of the PLCS group were significantly ($p < 0.05$) lower than those at the corresponding time points for the SHCS group (Fig. 3b). Furthermore, the SHCS biowastes treated cells showed no significant difference when compared to the data on normal cells reported by Yao *et al.*[65] The biowastes released from the myoblasts damaged under PLCS could significantly weaken the capability of the otherwise normal myoblasts to resist compressive damage, while the biowastes secreted from myoblasts damaged under SHCS did not show such effect significantly. The parameters from curve-fitting the experimental damage thresholds of compressive stress versus tolerance duration were shown in Table 2 for the PLCS and SHCS groups. The compressive damage stress-duration threshold of muscle cells after biowastes treatments could be described as below:

$$\sigma_B = \frac{347}{1 + e^{0.0527(t-54.7)}} + 10.83 \qquad (9)$$

The compressive damage thresholds at loading duration 70 min of myoblasts treated by biowastes collected from damaged myoblasts in SHCS, PHCS,

TABLE 2. The model parameters obtained from curve-fitting the experimental results of the PLCS and the SHCS biowastes treated groups using the sigmoid function represented by Eq. (1), as compared to the non-treated myoblasts.[64]

	K (Pa)	α (min^{-1})	C(Pa)	t_0 (min)	R^2
Non-treated myoblasts	340.0	0.118	8.95	160.3	0.991
PLCS biowastes treated myoblasts	347.6	0.0527	10.83	54.7	0.988
SHCS biowastes treated myoblasts	323.5	0.154	3.48	157.7	0.993

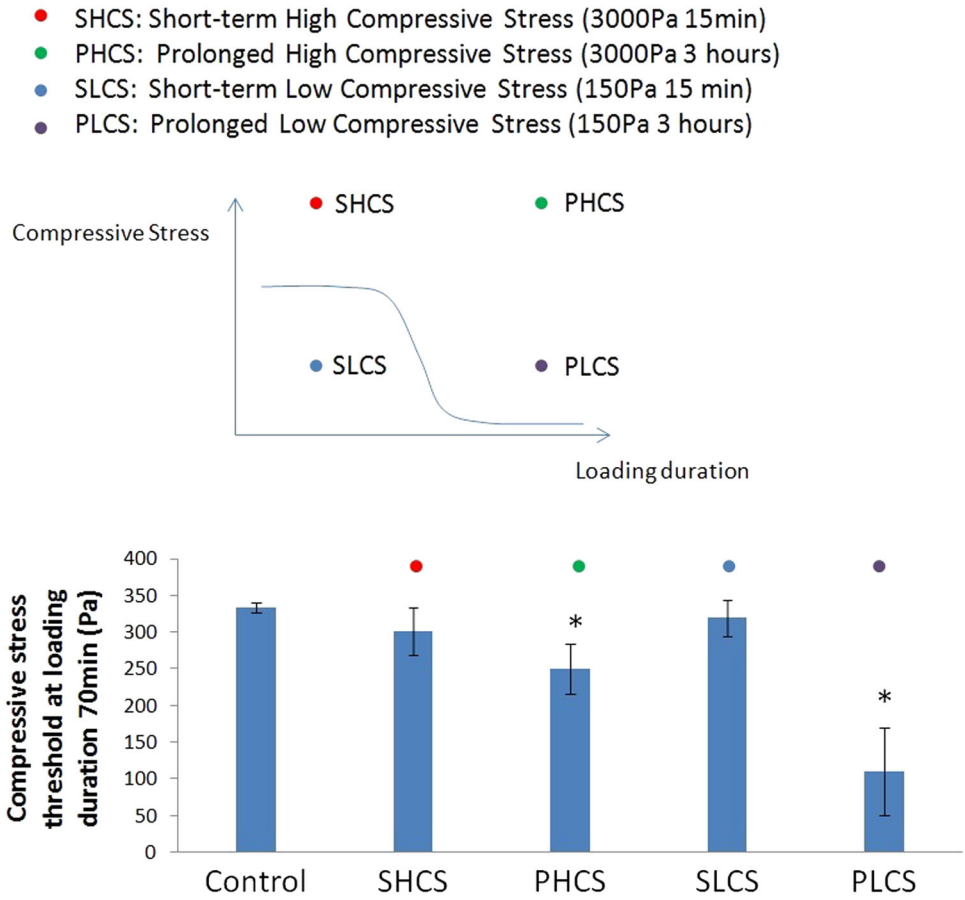

FIGURE 4. Two-way ANOVA showed that loading duration apparently had a significant effect on the toxicity of the biowastes generated from the damaged myoblasts, which in turn led to a significant change in the compressive damage threshold of the myoblasts. (*$p < 0.05$).

SLCS and PLCS groups were shown in Fig. 4. Two-way ANOVA with Tukey's post hoc test showed that loading duration was the main factor that influenced the effect of biowastes secreted from the damaged muscle cells. Cell damage caused by short loading duration could not generate biowastes as toxic as those from prolonged loading duration. Cell damage caused by prolonged loading could generate biowastes that could lower the compressive damage stress-duration threshold of normal myoblasts. We assumed a loading duration of 2 h was enough to cause the loaded muscle cells to release significantly toxic biowastes to its immediate vicinity, as the compressive damage stress-duration threshold curve of normal myoblasts started to drop sharply at around 2 h.[65]

COMSOL Multiphysics Simulation

The distributions of minimum principal stress in the buttock-cushion system and in the muscle layer were shown in Fig. 5. The compressive stress was highest at the site in the muscle layer beneath the IT bone, which was most vulnerable to damage. The release of toxic biowastes was determined by the compressive damage

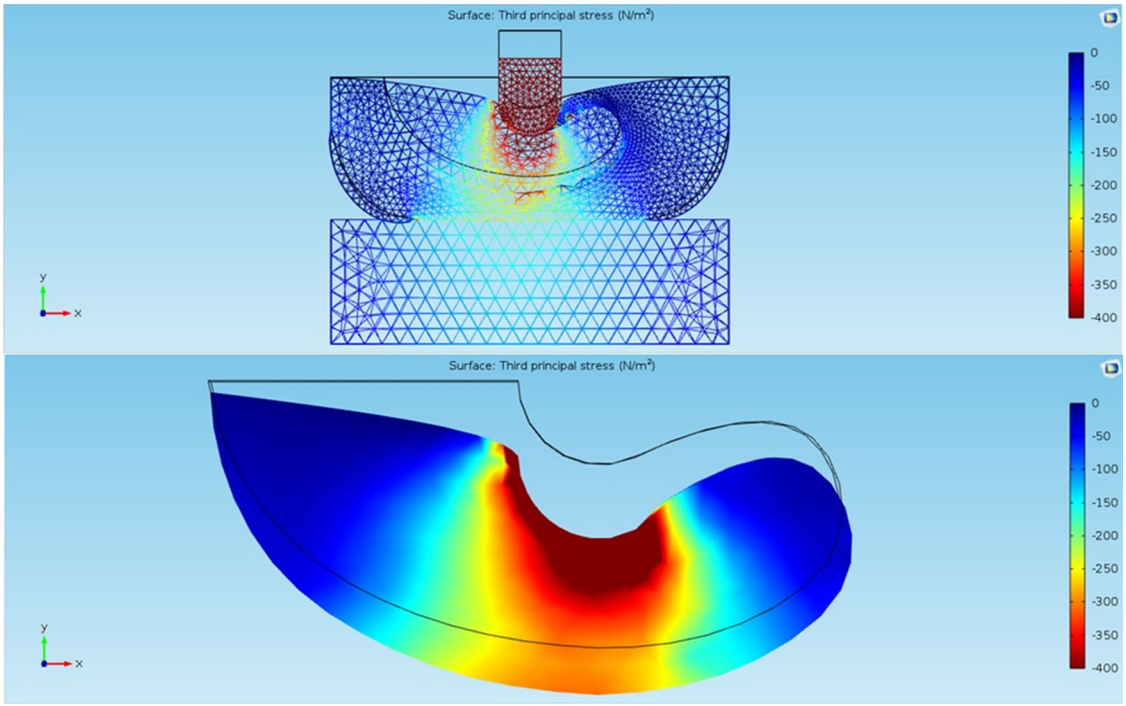

FIGURE 5. Distribution of minimum principal stress in the buttock-cushion system (upper figure) and in the muscle tissue (lower figure).

stress-duration threshold of muscle cells could in-turn change the compressive damage threshold of the muscle cells in the neighborhood. The patterns of propagation of muscle damage with and without the biowastes effect were simulated using the reference parameters ($D = 10^{-9}$ m^2 s^{-1}; $R_C = 10^{-6}$ mol m^{-3} s^{-1}; $t_0 = 120$ min; $C_t = 0$ mol m^{-3}) and the results were shown in Fig. 6. The number of damaged elements (red area) in the muscle layer with the biowastes effect was larger than that without the biowastes effect in the time span of 2–3 h. The biowastes could worsen the tissue damage faster if they were not cleared from the tissues.

Figure 7a showed the comparison of the effects of different diffusion coefficients of the biowastes in the muscle layer with the release rate of the biowastes R; the chemical damage threshold C_t and timeline of releasing biowastes t_0 kept at the reference values. Larger diffusion coefficient of the biowastes could allow the biowastes diffuse faster to the whole muscle layer causing faster expansion of damage in the muscle tissue. When the diffusion coefficient reached 10^{-7} m^2 s^{-1}, the damage progression was not much affected by further increase in the diffusion coefficient. When there were toxic biowastes generated, even a small diffusion coefficient could cause more damage than the situation without biowastes.

The comparison of the effects of different release rates of biowastes was shown in Fig. 7b with the diffusion coefficient D; the chemical damage threshold C_t and timeline of releasing biowastes t_0 kept at the reference values. A higher release rate of biowastes could cause a faster expansion of muscle damage. When the release rate reached 10^{-5} mol m^{-3} s^{-1}, the damaged tissue volume was not much increased by further increase in the release rate.

The comparison of the effects of different chemical damage threshold of muscle cells against the toxic biowastes was shown in Fig. 7c with the diffusion coefficient D; the release rate R and timeline of releasing biowastes t_0 kept at the reference values. A higher chemical damage threshold against the toxic biowastes could slow down the effects of biowastes on the damage expansion.

With an earlier time point when the damaged cells could release their biowastes, the effects of the biowastes on the damage expansion will be advanced (Fig. 7d), with the diffusion coefficient D; the release rate R and the chemical damage threshold C_t kept at the reference values.

DISCUSSION

From the results in Figs. 2a and 2b, the PLCS biowastes were different from the SHCS biowastes. The PLCS biowastes were clearly toxic to normal myoblasts while the SHCS biowastes appeared not so. The biowastes released from myoblasts under prolonged low compressive loading might contain cytokines, caspases and ROS which are known to be

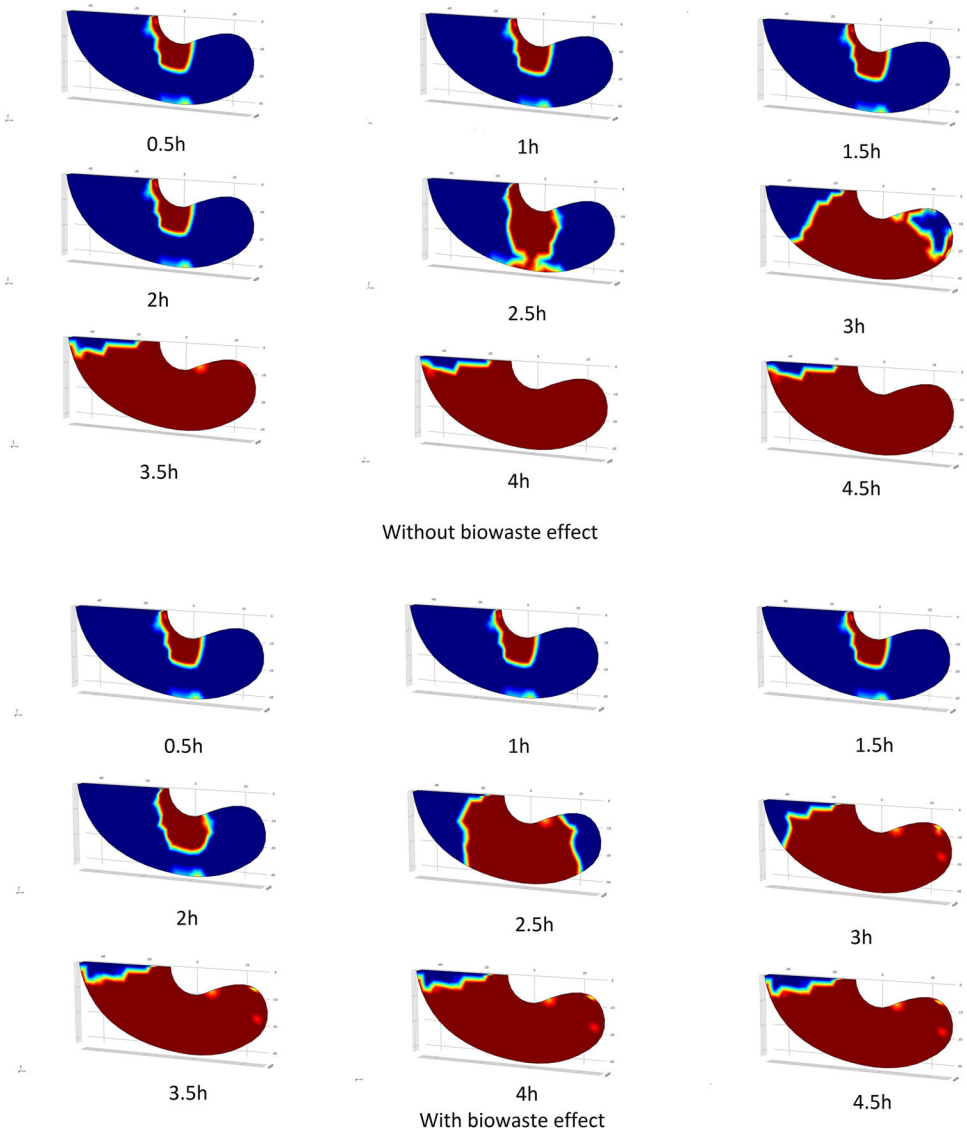

FIGURE 6. Evolution of damage (red area) in the muscle tissue under prolonged skeletal loading with and without the effect of biowastes, using reference parameters, $D = 10^{-9}$ m^2 s^{-1}; $R_C = 10^{-6}$ mol m^{-3} s^{-1}; $t_0 = 120$ min; $C_t = 0$ mol m^{-3}.

toxic to cells and can affect the mechanical properties of cells. Cells under PLCS apparently responded by producing toxic biowastes. Such toxic biowastes could be released and diffused to the surrounding, compromising other cells in the neighborhood. On the other hand, high compressive stress could rupture cells causing cell deaths immediately before a significant amount of toxic biowastes could be generated. The compressive damage stress-duration threshold of normal myoblasts[65] showed that a compressive stress of 3000 Pa could cause cell death immediately. Such loading for 15 min might not give enough time for cells to respond *via* signaling pathways to produce harmful biowastes with apoptotic agonists, toxic cytokines, and ROS.

Increased cell damage with the increase of indentation duration was observed in both PLCS and SHCS biowastes treated samples (Table 1). PLCS biowastes compromised cell viability under compressive stress. The tolerance of myoblasts against compressive damage after PLCS biowastes treatments appeared to be significantly decreased after around 50 min of loading (Table 2), which was much faster than those of the SHCS biowastes treated myoblasts (Fig. 3b) and the normal myoblasts.[65] PLCS biowastes could cause earlier breakdown of cell membranes under compres-

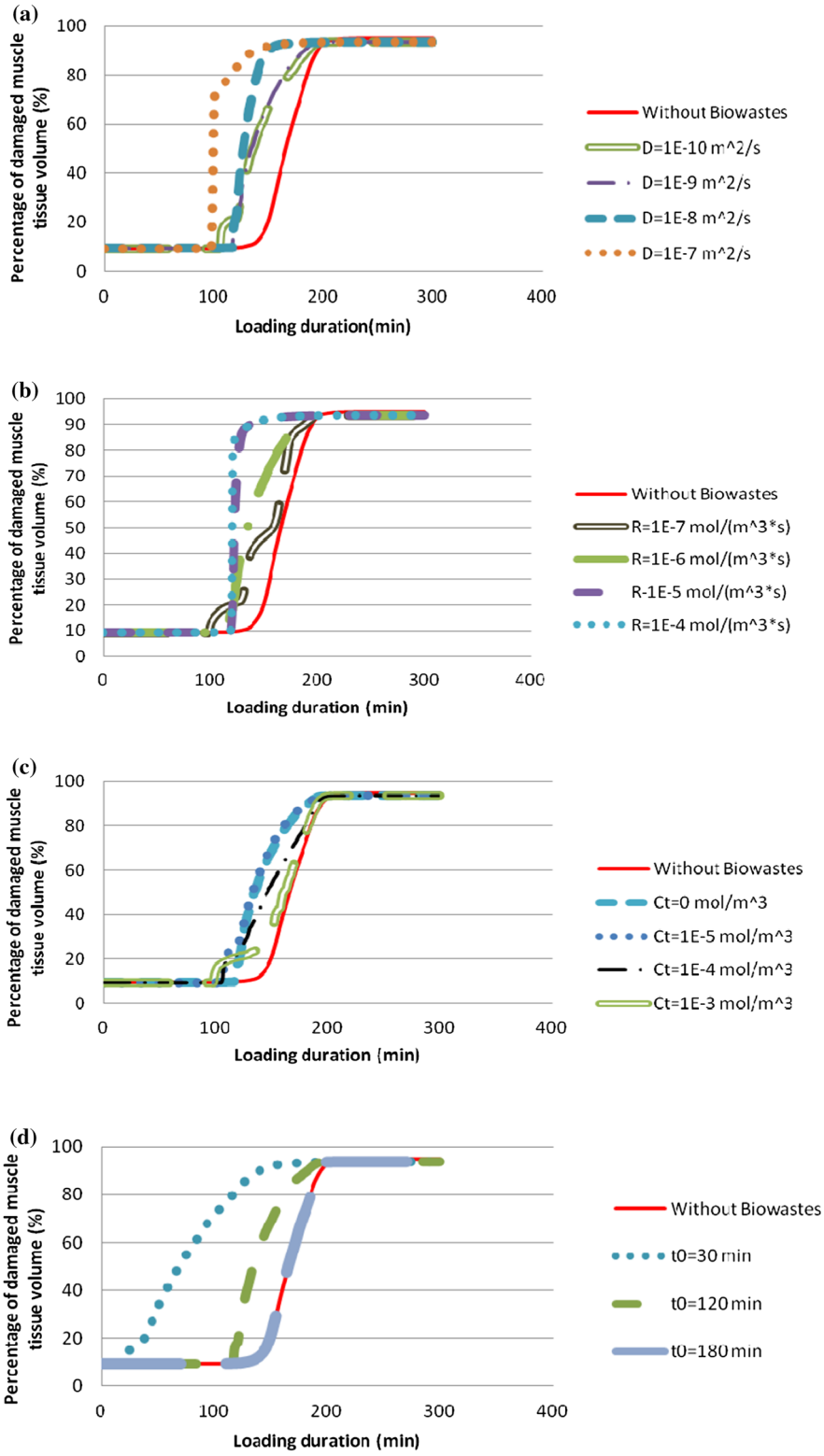

FIGURE 7. (a) Larger diffusion coefficient of biowastes in the muscle tissue, (b) higher release rate of biowastes from damaged muscle cells, (c) lower chemical damage threshold of muscle cells against biowastes, and (d) earlier timeline of releasing biowastes of muscle cells leads to earlier expansion of muscle damage under prolonged skeletal loading.

sive stress than SHCS biowastes and normal culture media. The mechanical strength of cells decreased with loading duration and could be further compromised by the accumulated biowastes released from other neighboring cells that had succumbed earlier to the prolonged mechanical challenge. In contrast, myoblasts undergoing acute cell death might not as much affect the neighboring cells *via* the biowastes released upon their abrupt ruptures.

The results implied that the accumulated biowastes released from the muscle cells damaged under PLCS can compromise the capability of the remaining cells to withstand the subsequent mechanical damages. The accumulation of biowastes *in vivo* could also be caused by blocked lymphatic drainages due to tissue deformation under mechanical loading. The inability of the compromised lymphatics to drain the toxic biowastes could further harm the remaining intact cells.

A major assumption in the *in silico* study is that the model was established as a 3D thin slice rather than a full-3D model. The anterior and posterior surface of the geometry were assumed be free in-plane and fixed out-of-plane, which might exaggerate the compressive stress value. The highest internal compressive stress in the muscle was found, as expected, below the IT bone. Tissue damage initiated around the bony prominence. Both were similar to those reported in previous studies.[36,64] Direct comparisons in terms of absolute values were not further pursued, due to differences in the details of the models. We recommend that the predictions of the present *in silico* model be interpreted as trends of the biowastes effects, and not necessarily in terms of their absolute values, since the damage laws were based only on our *in vitro* data. A full 3D model would still be required if the effects of out-of-plane need to be further elucidated.

Results from the multiphysics FE modeling illustrated the effect of the biowastes generated by damaged muscle tissue on the propagation of tissue damage. This implication is relevant to the development of clinical pressure ulcers from DTI. The biowastes could cause faster tissue damage if the biowastes cannot be timely removed. The estimated diffusion coefficient of biowastes in the uncompressed muscle tissue ranged from 0.83 to 1.22×10^{-9} m^2 s^{-1}.[2,11,19,58,59] In human lower limb, the mean diffusion coefficient in skeletal muscle were reportedly in the range of $1.31–1.41 \times 10^{-9}$ m^2 s^{-1}.[66] Parametric analysis of the diffusion coefficient indicated that with an increase of diffusion coefficient, the propagation of muscle damage became faster. The imbalance between capillary filtration and lymph drainage could cause tissue edema which might be developed in DTI.[40] The tissue edema could increase the diffusion coefficient.[13] During the development of DTI, the edema could make the tissue damage more severe through faster diffusion of biowastes. *In vitro* study revealed that free diffusion of large molecules (10–150 kDa) decreased during deformation.[16] *In vivo* study showed the diffusion of small molecules was not influenced by deformation of muscle tissue, but the observed decrease in diffusion coefficient was associated with a decrease of muscle temperature.[59] The diffusion coefficient during the development of DTI might vary but the damage propagation changed little when the diffusion coefficient was less than 10^{-9} m^2 s^{-1}. Damage propagation was sensitive to the diffusion coefficient larger than 10^{-9} m^2 s^{-1}. Real-time measurement of diffusion coefficient during the development of DTI could support the multiphysics simulation with more accurate parameters. Figure 7b indicated faster release of biowastes from the cells to the surrounding could cause more severe tissue damage. Blockage of lymphatic system might significantly inhibit the removal of biowastes in the tissue and thus increase the accumulation of biowastes leading to faster damage. The muscle tissue might be tolerant to biowastes up to certain biowastes concentration, above which, the muscle tissue would find it difficult to cope with. Figure 7c indicated that a higher chemical damage threshold of the muscle tissue against the biowastes could help slow down the effects of biowastes on the propagation of damage. Figure 7d indicated the timeline of releasing biowastes from muscle cells were important to the beginning of the damage propagation which might be guide for the clinical need of repositioning frequency of vulnerable patients to prevent DTI. *In silico* model indicated the biowastes could lead to faster or earlier propagation of damage in the muscle tissue, and thus biowastes accumulation and *in vivo* tissue diffusion coefficient could be important factors related to pressure ulcer development from DTI.

The *in vitro* experiments revealed the importance of biowastes which could be cytotoxic and could compromise the capability of intact normal cells to resist compressive damage. Although the multi-physics simulation in this study is a big step from the cellular level to tissue level, it does suggest the potential relevance of the timing and rate of release and the subsequent diffusion of these biowastes to the clinical development of DTI.

There were few literature reports on the exact compositions of the biowastes released by muscle cells damaged under mild but prolonged mechanical insults, nor on the general biochemical environment in the tissues at risk of DTI *in vivo*. We have raised the issue of biowastes accumulation under prolonged mild mechanical loading as a potentially important factor in the etiology of DTI. Strategies that could lead to a

decrease in the production of toxic biowastes, timely removal of the toxic biowastes through in situ neutralization, or blunting the cell receptors of the toxic proteins in the biowastes could be explored as potential interventions to prevent the clinical development of DTI. The identification and quantification of the major toxins in the biowastes released from muscle cells under prolonged mild loading would be essential to the development of these strategies.

ACKNOWLEDGMENTS

This study was supported by Hong Kong Research Grant Council (RGC Ref. No.: CUHK415413).

CONFLICT OF INTEREST

No conflict of interest.

REFERENCES

[1]Bader, D. L., C. Bouten, D. Colin, and C. W. J. Oomens. Pressure Ulcer Research: Current and Future Perspectives. New York: Springer, 2005.
[2]Basser, P. J., J. Mattiello, and D. LeBihan. MR diffusion tensor spectroscopy and imaging. *Biophys. J.* 66(1):259, 1994.
[3]Bliss, M. R. Aetiology of pressure sores. *Rev. Clin. Gerontol.* 3(04):379–397, 1993.
[4]Bogie, K. M., I. Nuseibeh, and D. L. Bader. Early progressive changes in tissue viability in the seated spinal cord injured subject. *Spinal Cord* 33(3):141–147, 1995.
[5]Bouten, C. V., M. M. Knight, D. A. Lee, and D. L. Bader. Compressive deformation and damage of muscle cell subpopulations in a model system. *Ann. Biomed. Eng.* 29(2):153–163, 2001.
[6]Breuls, R. G. M., C. V. C. Bouten, C. W. J. Oomens, D. L. Bader, and F. P. T. Baaijens. Compression induced cell damage in engineered muscle tissue: an *in vitro* model to study pressure ulcer aetiology. *Ann. Biomed. Eng.* 31(11):1357–1364, 2003.
[7]Byrne, D. W., and C. A. Salzberg. Major risk factors for pressure ulcers in the spinal cord disabled: a literature review. *Spinal Cord* 34:255–263, 1996.
[8]Cheng, W., B. Li, J. Kajstura, P. Li, M. S. Wolin, E. H. Sonnenblick, T. H. Hintze, G. Olivetti, and P. Anversa. Stretch-induced programmed myocyte cell death. *J. Clin. Investig.* 96(5):2247, 1995.
[9]Comley, K., and N. A. Fleck. The high strain rate response of adipose tissue. In: IUTAM Symposium on Mechanical Properties of Cellular Materials (pp. 27–33). Springer, Netherlands, 2009.
[10]Comley, K., and N. A. Fleck. A micromechanical model for the Young's modulus of adipose tissue. *Int. J. Solids Struct.* 47(21):2982–2990, 2010.
[11]Damon, B. M., Z. Ding, A. W. Anderson, A. S. Freyer, and J. C. Gore. Validation of diffusion tensor MRI-based muscle fiber tracking. *Magn. Reson. Med.* 48(1):97–104, 2002.
[12]Elsner, J. J., and A. Gefen. Is obesity a risk factor for deep tissue injury in patients with spinal cord injury? *J. Biomech.* 41(16):3322–3331, 2008.
[13]Fan, R. H., and M. D. Does. Compartmental relaxation and diffusion tensor imaging measurements *in vivo* in λ-carrageenan-induced edema in rat skeletal muscle. *NMR Biomed.* 21(6):566–573, 2008.
[14]Frost, R. A., C. H. Lang, and M. C. Gelato. Transient exposure of human myoblasts to tumor necrosis factor-α inhibits serum and insulin-like growth factor-I stimulated protein synthesis 1. *Endocrinology* 138(10):4153–4159, 1997.
[15]Gawlitta, D., W. Li, C. W. J. Oomens, F. P. Baaijens, D. L. Bader, and C. V. Bouten. The relative contributions of compression and hypoxia to development of muscle tissue damage: an *in vitro* study. *Ann. Biomed. Eng.* 35(2):273–284, 2007.
[16]Gefen, A., L. H. Cornelissen, D. Gawlitta, D. L. Bader, and C. W. Oomens. The free diffusion of macromolecules in tissue-engineered skeletal muscle subjected to large compression strains. *J. Biomech.* 41(4):845–853, 2008.
[17]Gefen, A., and E. Haberman. Viscoelastic properties of ovine adipose tissue covering the gluteus muscles. *J. Biomech. Eng.* 129(6):924–930, 2007.
[18]Greiwe, J. S., B. O. Cheng, D. C. Rubin, K. E. Yarasheski, and C. F. Semenkovich. Resistance exercise decreases skeletal muscle tumor necrosis factor α in frail elderly humans. *FASEB J.* 15(2):475–482, 2001.
[19]Heemskerk, A. M., G. J. Strijkers, M. R. Drost, G. S. van Bochove, and K. Nicolay. Skeletal muscle degeneration and regeneration after femoral artery ligation in mice: monitoring with diffusion MR imaging 1. *Radiology* 243(2):413–421, 2007.
[20]Heidlauf, T., and O. Röhrle. Modeling the chemoelectromechanical behavior of skeletal muscle using the parallel open-source software library OpenCMISS. *Comput. Math. Methods Med.* 2013:517287, 2013.
[21]Henkel, J. S., D. R. Beers, W. Zhao, and S. H. Appel. Reactive Oxygen and Nitrogen Species—A Driving Force in Amyotrophic Lateral Sclerosis. Systems Biology of Free Radicals and Antioxidants. Berlin: Springer, pp. 3141–3165, 2014.
[22]Hsieh, M. H., and H. T. Nguyen. Molecular mechanism of apoptosis induced by mechanical forces. *Int. Rev. Cytol.* 245:45–90, 2005.
[23]Joda, A., Z. Jin, A. Haverich, J. Summers, and S. Korossis. Multiphysics simulation of the effect of leaflet thickness inhomogeneity and material anisotropy on the stress–strain distribution on the aortic valve. *J. Biomech.* 2016. doi: 10.1016/j.jbiomech.2016.02.041.
[24]Kang, I., D. Panneerselvam, V. P. Panoskaltsis, S. J. Eppell, R. E. Marchant, and C. M. Doerschuk. Changes in the hyperelastic properties of endothelial cells induced by tumor necrosis factor-α. *Biophys. J.* 94(8):3273–3285, 2008.
[25]Krouskop, T. A. A synthesis of the factors that contribute to pressure sore formation. *Med. Hypotheses* 11:255–267, 1983.
[26]Lemaire, T., J. Kaiser, S. Naili, and V. Sansalone. Three-scale multiphysics modeling of transport phenomena within cortical bone. *Math. Probl. Eng.* 2015. doi:10.1155/2015/398970.
[27]Leopold, E., and A. Gefen. Stretching affects intracellular oxygen levels: three-dimensional multiphysics studies. *J. Biomech. Eng.* 134(6):064501, 2012.

[28]Leopold, E., R. Sopher, and A. Gefen. The effect of compressive deformations on the rate of build-up of oxygen in isolated skeletal muscle cells. *Med. Eng. Phys.* 33(9):1072–1078, 2011.
[29]Leri, A., Y. Liu, B. Li, F. Fiordaliso, A. Malhotra, R. Latini, J. Kajstura, and P. Anversa. Up-regulation of AT 1 and AT 2 receptors in postinfarcted hypertrophied myocytes and stretch-mediated apoptotic cell death. *Am. J. Pathol.* 156(5):1663–1672, 2000.
[30]Ley, O., and T. Kim. Calculation of arterial wall temperature in atherosclerotic arteries: effect of pulsatile flow, arterial geometry, and plaque structure. *Biomed Eng Online* 6(8):1, 2007.
[31]Li, Y., and M. B. Reid. Effect of tumor necrosis factor-α on skeletal muscle metabolism. *Curr. Opin. Rheumatol.* 13(6):483–487, 2001.
[32]Li, Y. P., and R. J. Schwartz. TNF-α regulates early differentiation of C2C12 myoblasts in an autocrine fashion. *FASEB J.* 15(8):1413–1415, 2001.
[33]Lim, D., F. Lin, R. W. Hendrix, B. Moran, C. Fasanati, and M. Makhsous. Evaluation of a new sitting concept designed for prevention of pressure ulcer on the buttock using finite element analysis. *Med. Biol. Eng. Comput.* 45(11):1079–1084, 2007.
[34]Linder-Ganz, E., S. Engelberg, M. Scheinowitz, and A. Gefen. Pressure–time cell death threshold for albino rat skeletal muscles as related to pressure sore biomechanics. *J. Biomech.* 39(14):2725–2732, 2006.
[35]Linder-Ganz, E., and A. Gefen. Mechanical compression induced pressure sores in rat hindlimb: muscle stiffness, histology, and computational models. *J. Appl. Physiol.* 96:2034–2049, 2004.
[36]Linder-Ganz, E., and A. Gefen. Stress analyses coupled with damage laws to determine biomechanical risk factors for deep tissue injury during sitting. *J. Biomech. Eng.* 131(1):011003, 2009.
[37]Linder-Ganz, E., N. Shabshin, Y. Itzchak, and A. Gefen. Assessment of mechanical conditions in sub-dermal tissues during sitting: a combined experimental-MRI and finite element approach. *J. Biomech.* 40(7):1443–1454, 2007.
[38]Linder-Ganz, E., G. Yarnitzky, Z. Yizhar, I. Siev-Ner, and A. Gefen. Real-time finite element monitoring of sub-dermal tissue stresses in individuals with spinal cord injury: toward prevention of pressure ulcers. *Ann. Biomed. Eng.* 37:387–400, 2009.
[39]Mak, A. F. T., Y. Y. Yu, L. P. C. Kwan, L. Sun, and E. W. C. Tam. Deformation and reperfusion damages and their accumulation in subcutaneous tissues during loading and unloading: a theoretical modeling of deep tissue injuries. *J. Theor. Biol.* 289:65–73, 2011.
[40]Mak, A. F., M. Zhang, and E. W. Tam. Biomechanics of pressure ulcer in body tissues interacting with external forces during locomotion. *Annu. Rev. Biomed. Eng.* 12:29–53, 2010.
[41]Makhsous, M., D. Lim, R. Hendrix, J. Bankard, W. Z. Rymer, and F. Lin. Finite element analysis for evaluation of pressure ulcer on the buttock: development and validation. *IEEE Trans. Neural Syst. Rehabil. Eng.* 15(4):517–525, 2007.
[42]Miller, G. E., and J. L. Seake. The recovery of terminal lymph flow following occlusion. *J. Biomed. Eng.* 109:48–54, 1987.
[43]Oomens, C. W. J., S. Loerakker, and D. L. Bader. The importance of internal strain as opposed to interface pressure in the prevention of pressure related deep tissue injury. *J. Tissue Viability* 19(2):35–42, 2010.
[44]Oomens, C. W. J., M. Maenhout, C. H. Van Oijen, M. R. Drost, and F. P. Baaijens. Finite element modelling of contracting skeletal muscle. *Philos. Trans. R. Soc. Lond. B Biol. Sci.* 358(1437):1453–1460, 2003.
[45]Palevski, A., I. Glaich, S. Portnoy, E. Linder-Ganz, and A. Gefen. Stress relaxation of porcine gluteus muscle subjected to sudden transverse deformation as related to pressure sore modeling. *J. Biomech. Eng.* 128(5):782–787, 2006.
[46]Peake, J., P. Della Gatta, K. Suzuki, and D. Nieman. Cytokine expression and secretion by skeletal muscle cells: regulatory mechanisms and exercise effects. *Exerc. Immunol. Rev.* 21:8–25, 2015.
[47]Pedersen, B. K. Muscular interleukin-6 and its role as an energy sensor. *Med. Sci. Sports Exerc.* 44(3):392–396, 2012.
[48]Pelling, A. E., F. S. Veraitch, C. P. Chu, B. M. Nicholls, A. L. Hemsley, C. Mason, and M. A. Horton. Mapping correlated membrane pulsations and fluctuations in human cells. *J. Mol. Recognit.* 20(6):467–475, 2007.
[49]Reddy, N. P. Effects of Mechanical Stresses on Lymph and Interstitial Fluid Flow. Pressure Sores: Clinical Practice and Scientific Approach. London: Macmillan, pp. 203–220, 1990.
[50]Ruschkewitz, Y., and A. Gefen. Cell-level temperature distributions in skeletal muscle post spinal cord injury as related to deep tissue injury. *Med. Biol. Eng. Comput.* 48(2):113–122, 2010.
[51]Siu, P. M., E. W. Tam, B. T. Teng, X. M. Pei, J. W. Ng, I. F. Benzi, and A. F. Mak. Muscle apoptosis is induced in pressure-induced deep tissue injury. *J. Appl. Physiol.* 107:1266–1275, 2009.
[52]Slomka, N., and A. Gefen. Relationship between strain levels and permeability of the plasma membrane in statically stretched myoblasts. *Ann. Biomed. Eng.* 40(3):606–618, 2012.
[53]Slomka, N., S. Or-Tzadikario, D. Sassun, and A. Gefen. Membrane-stretch-induced cell death in deep tissue injury: computer model studies. *Cell Mol. Bioeng.* 2(1):118–132, 2009.
[54]Solis, L. R., A. Liggins, R. R. Uwiera, N. Poppe, E. Pehowich, P. Seres, R. B. Thompson, and V. K. Mushahwar. Distribution of internal pressure around bony prominences: implications to deep tissue injury and effectiveness of intermittent electrical stimulation. *Ann. Biomed. Eng.* 40(8):1740–1759, 2012.
[55]Taylor, R. C., S. P. Cullen, and S. J. Martin. Apoptosis: controlled demolition at the cellular level. *Nat. Rev. Mol. Cell Biol.* 9(3):231–241, 2008.
[56]Tham, L. M., H. P. Lee, and C. Lu. Cupping: from a biomechanical perspective. *J. Biomech.* 39(12):2183–2193, 2006.
[57]Tsivitse, S. K., E. Mylona, J. M. Peterson, W. T. Gunning, and F. X. Pizza. Mechanical loading and injury induce human myotubes to release neutrophil chemoattractants. *Am. J. Physiol. Cell Physiol.* 288(3):C721–C729, 2005.
[58]Van Donkelaar, C. C., L. J. G. Kretzers, P. H. M. Bovendeerd, L. M. A. Lataster, K. Nicolay, J. D. Janssen, and M. R. Drost. Diffusion tensor imaging in biomechanical studies of skeletal muscle function. *J. Anat.* 194(1):79–88, 1999.
[59]Van Nierop, B. J., A. Stekelenburg, S. Loerakker, C. W. Oomens, D. Bader, G. J. Strijkers, and K. Nicolay. Diffusion of water in skeletal muscle tissue is not influenced by

compression in a rat model of deep tissue injury. *J. Biomech.* 43(3):570–575, 2010.
[60]Verver, M. M., J. Van Hoof, C. W. J. Oomens, J. S. H. M. Wismans, and F. P. T. Baaijens. A finite element model of the human buttocks for prediction of seat pressure distributions. *Comput. Methods Biomech. Biomed. Eng.* 7(4):193–203, 2004.
[61]Vilcek, J., and T. H. Lee. Tumor necrosis factor. New insights into the molecular mechanisms of its multiple actions. *J. Biol. Chem.* 266(12):7313–7316, 1991.
[62]Wójciak-Stothard, B., A. Entwistle, R. Garg, and A. J. Ridley. Regulation of TNF-α-induced reorganization of the actin cytoskeleton and cell-cell junctions by Rho, Rac, and Cdc42 in human endothelial cells. *J. Cell. Physiol.* 176(1):150–165, 1998.
[63]Wong, S. W., S. Sun, M. Cho, K. K. Lee, and A. F. T. Mak. H_2O_2 exposure affects myotube stiffness and actin filament polymerization. *Ann. Biomed. Eng.* 43(5):1178–1188, 2015.
[64]Xiao, D. Z., S. Y. Wu, and A. F. Mak. Accumulation of loading damage and unloading reperfusion injury—modeling of the propagation of deep tissue ulcers. *J. Biomech.* 47(7):1658–1664, 2014.
[65]Yao, Y., Z. Xiao, S. Wong, Y. C. Hsu, T. Cheng, C. C. Chang, L. Bian, and A. F. Mak. The effects of oxidative stress on the compressive damage thresholds of C_2C_{12} mouse myoblasts: implications for deep tissue injury. *Ann. Biomed. Eng.* 43(2):287–296, 2015.
[66]Zaraiskaya, T., D. Kumbhare, and M. D. Noseworthy. Diffusion tensor imaging in evaluation of human skeletal muscle injury. *J. Magn. Reson. Imaging* 24(2):402–408, 2006.
[67]Zhang, Y., G. Pilon, A. Marette, and V. E. Baracos. Cytokines and endotoxin induce cytokine receptors in skeletal muscle. *Am. J. Physiol. Endocrinol. Metab.* 279(1):E196–E205, 2000.